energies

MDPI

Article

Multi-Objective Optimization of a Heat Sink for the Thermal Management of a Peltier-Cell-Based Biomedical Refrigerator

Lorenzo Gragnaniello [1], Marcello Iasiello [2,*] and Gerardo Maria Mauro [3]

[1] Carpitech Srl, Via Coroglio 54, 80124 Napoli, Italy
[2] Dipartimento di Ingegneria Industriale, Università degli Studi di Napoli Federico II, P. Le Tecchio 80, 80125 Napoli, Italy
[3] Dipartimento di Ingegneria, Università degli Studi del Sannio, Piazza Roma 21, 82100 Benevento, Italy
* Correspondence: marcello.iasiello@unina.it

Abstract: Both storage and transport of medical products remains a challenging task because of many variables as well as infrastructures, territory, and so on. Among these variables, monitoring the medical products temperature is fundamental to guarantee their safety. On the other hand, for sectors like aerospace delivery, weight has a crucial role too. For such applications and especially for strongly variable external temperatures, Peltier cells might be employed for either cooling or heating medical products to be stored. Accordingly, this study addresses the optimization of a heat sink for the thermal management of a Peltier-cell-based biomedical refrigerator. In detail, a brute-force multi-objective optimization of an impinging-flow finned heat sink for the Peltier cell is carried out here. Thermal resistance, weight, and pressure drop are chosen as the three-objective functions to be minimized, with both geometrical and volumetric flow rate as design variables. The results present a very large bunch of optimal solutions to design such devices. With the utopia optimum criterion, R_{th} = 0.159 °C/W, m_{sink} = 0.550 kg, and Δp = 14.99 Pa are obtained. Finally, both multiple-linear regression and artificial neural networks are employed to relate design variables with the objective functions, in order to provide the final user with a practical tool for the optimal design of such devices.

Keywords: thermal management; Peltier cells; multi-objective optimization; heat transfer and pressure drop; correlations

Citation: Gragnaniello, L.; Iasiello, M.; Mauro, G.M. Multi-Objective Optimization of a Heat Sink for the Thermal Management of a Peltier-Cell-Based Biomedical Refrigerator. *Energies* **2022**, *15*, 7352. https://doi.org/10.3390/en15197352

Academic Editor: Dimitrios Katsaprakakis

Received: 15 September 2022
Accepted: 3 October 2022
Published: 6 October 2022

1. Introduction

Storing goods related to medicine is a very complicated task because of the highly restricting conditions at which these should be maintained [1–3]. For instance, among all the variables, temperature is one of the most critical [1–3]. Depending on the organ, the drug, or in general on the biomedical product to be considered, different temperature ranges have to be considered. Some products like pads for back pain range in between 42 to 46 °C, while other ones like vaccines, or other clinical samples, should be in between 2/8 °C or 30/35 °C, respectively [3]. Some cells like peripheral blood mononuclear cells could be stored at −80 °C [4], or at −170 °C if one wants to avoid rapid deterioration [5]. Other products that require a controlled temperature environment are syrups, say no more than 25 °C [6], or some mRNA-based vaccines which require temperatures up to −80 °C or −20 °C [7]. If one wants to store epithelial cells for tissue engineering, then it is known that these could be of 2 °C up to 37 °C [8]. All this means that a very efficient thermal management solution is usually required.

Because heating or cooling might be required [3], solutions like heat pumps, Phase Change Materials (PCMs), or Peltier cells, might be some options. PCMs are efficient because of their ability to store very large amounts of thermal energy in isothermal conditions. This makes such materials very prone to these applications because PCMs can be chosen depending on the desired temperature range [3]; nowadays, applying these

materials within the biomedical industry, is something that is still of large interest [9,10]. Risk of vaccine freezing might be avoided if one uses PCMs [11]. A prototype to treat mycobacterium ulceran infection based on PCM has been shown to be promising since the PCM allows to keep the skin surface temperature up to 40 °C during the treatment, making possible to heal wounds with no other interventions [12]. Vaccine boxes might be prepared based on PCMs, since water presents too much of a low solidification temperature. If well designed, these boxes are also promising in terms of costs [3,13,14]. An exhaustive review of how to apply PCMs in biomedical field can be found in [15]. However, even if PCMs are essentially passive systems, they could present some issues in terms of weight, and of course in terms of thermal management since no forced convection systems are employed as for instance happens in electronic thermal management. Weight might be an issue especially in very remote areas that require the help of aircraft systems, water systems, or similar.

In order to overcome this limit, an idea could be to use Peltier cells, which can guarantee both cooling and heating as for a heat pump. Even if they present quite low coefficients of performance (COP) values, these might be thought for rural areas [16], to avoid any environmental degradation fluids [16,17], or refrigerant leakages [18]. During the very recent years, many studies suggested to use Peltier cells for thermal management. They can be used for automotive or space applications [19], electrical machines [20], integrated circuits [21], and so on. Therefore, even if conventional vapor compression systems are more efficient, one can therefore use Peltier cells for low-weight applications in which either cooling or heating is required. This solution could guarantee an active thermal management system instead of a passive one based on phase change materials. When Peltier cells are designed, their overall performance is improved if a proper design of the corresponding heat sink for both cold and hot sides is done [16–18]. To accomplish this task, multi-objective optimization would be really important. Multi-objective optimization has been extensively used for typical heat transfer problems such as heat exchangers [22], energy efficiency in buildings [23], or in general energy systems [24]. In this subject, one must decide which are the conflicting functions to be minimized/maximized in order to obtain a 2D or 3D Pareto front. Recently, many studies about optimization applied to heat transfer by employing various optimization techniques have been proposed. Various heat sinks for electronics have been optimized by employing water and HFE-7000 as coolants by Ndao et al. [25], addressing thermal resistance and pumping power as objective functions. Their study is a guideline for whom wants to design these heat transfer devices, showing that the offset strip fin heat sink might be the best solution for that application. A heat sink for concentrated PVT applications has been optimized by [26], by employing thermal resistance and pressure drop as objective functions. The authors concluded that variable-width channels might reduce cooling fluid pressure drop. Plate heat exchangers have been optimized in terms of hot side pressure drop and heat transfer rate [27] to show that some variables like place spacing and numbers would affect greatly both heat transfer and pressure drop. A heat rate and pumping power optimization for porous media-equipped heat sinks has been presented in Bianco et al. [28]. The mathematical model for the optimization has been set by numerically solving the 3D model with CFD analysis. Results showed that the optimized solution outperforms standard solutions [29] up to 5–6 times in terms of heat rate if one constraints pumping power.

Based on the current literature survey, it is clear that Peltier-based thermal management systems could be thought for low-weight applications. Since heat sinks in these applications have a primary role, in this study a multi-objective optimization of three contrasting objective functions which are thermal resistance, pressure drop and weight, is carried out. The optimization is carried out by employing a Brute-Force (BF) search, while the fitness function is built up based on available heat transfer and fluid flow correlations and simple geometrical considerations. Finally, correlations between design variables and objective functions are derived based on regression analysis and artificial neural network for whom wants to design such devices. The motivation of this study is that

optimizing these devices would be really helpful for whom wants to use Peltier-based thermal management systems. By considering the appropriate importance to heat transfer and fluid flow problem, reducing the weight would allow to carry on biomedical products by employing air shipping systems or in general solutions that are not as impactful as trucks and so on. Thus, optimizing such devices to trade-off thermal performance, weight and battery autonomy is pivotal to trigger a new, more effective and sustainable shipping system for essential goods, such as biomedical products, and non-essential goods, e.g., through unanimated air vehicles (UAV).

2. Mathematical Modeling

2.1. Geometry

The impinging-flow longitudinal finned heat sink that has been optimized here is sketched in Figure 1. The air comes from the top, i.e., the flow is impinging with respect to the heat source on the bottom of the heat sink. In the figure shown here, a number of N_{fins} = 32 fins, with w_w = 1.70 mm the fin thickness and w_c = 2.70 mm the fin spacing, is shown. The heat sink side L is always equal to 120 mm, the base H_b is 6.40 mm, while the height H is 33.6 mm in the figure, and it is assumed to be a design variable for the optimization.

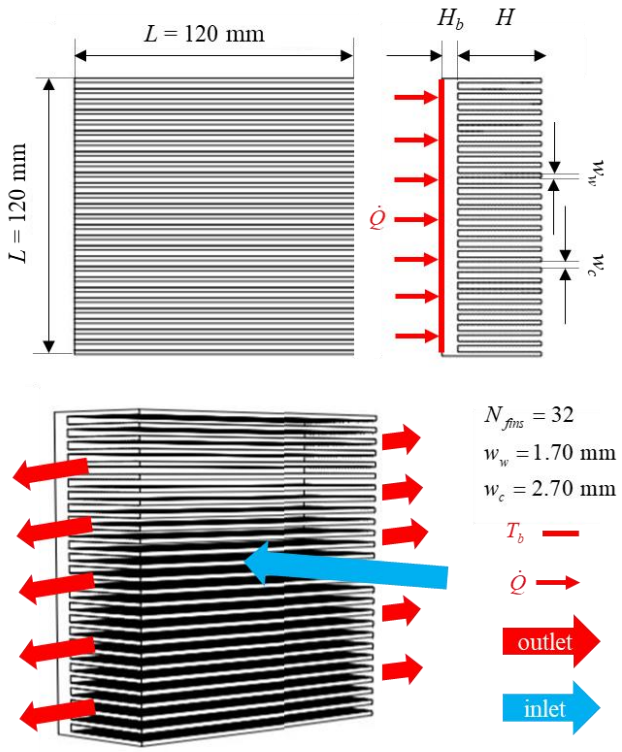

Figure 1. A sketch of the impinging-flow longitudinal finned heat sink to be optimized in this study.

2.2. Objective Functions

In order to define the optimization problem that will be shown later, both objective and fitness functions, with the latter that allows to relate input with outputs, need to be defined first.

The three objective functions to be minimized, which are in contrast and of equal importance, are the thermal resistance, the pressure drop, and the weight of the device. The first objective function, R_{th}, has been chosen since the objective of a heat sink is to minimize this value, which means lower temperature differences at equal heat rate for instance. In other words, we would like to improve the thermal performance of the device. Pressure drop, Δp, has to be minimized in order to ensure that a limited pumping power is required in transient conditions, resulting in savings in terms of battery consumption for

aircraft applications. In convection application, pressure drop is usually in contrast with heat transfer, that here is represented by the thermal resistance. Finally, the weight m_{sink} has been considered too, since it has a primary role in Peltier-based thermal management applications. Indeed, these devices might be convenient with references to applications like air shipping. This objective function is in contrast with the thermal resistance since if one wants to improve R_{th} then more material might be needed. On the other hand, the weight shows contrasting objectives with pressure drop since the latter is influenced by the material employed by means of fluid-dynamic variables like available cross section for flow and so on. Furthermore, lowering the heat sink weight would allow more space for batteries in applications unmanned aerial vehicles.

Thermal resistance and pressure drop have been taken from correlations shown in Kim et al. [30] for impinging plate-fin heat sinks:

$$R_{th} = \frac{\Delta T}{\dot{Q}} = \left\{ \varepsilon \rho_f c_{p,f} u_{in} L^2 \left[1 - \left(1 + \frac{\eta_{eff} h_c a_{sf} H}{\varepsilon \rho_f c_f u_{in}} \right)^{-1} \right] \right\}^{-1} \tag{1}$$

$$\Delta p = \rho_f u_{in} \left[\frac{1}{10} \left(\frac{L}{H} \right)^2 - \frac{2}{5} \right] + \frac{\varepsilon \mu_f H}{K} u_{in} \left[\frac{1}{12} \left(\frac{L}{H} \right)^2 + \frac{1}{3} \right] \tag{2}$$

With R_{th} as the thermal resistance, ΔT as the temperature difference between the base and the air inlet temperature, $\dot{Q}$ as the heat rate, e as the porosity, ρ as the density, $c_{p,f}$ as the heat capacity, u_{in} as the inlet velocity, h_c as the interfacial heat transfer coefficient, a_{sf} as the specific surface area, η_{eff} as the fin efficiency and K as the permeability. In this study, we assume that the heat sink is squared with L = 120 mm, while thermophysical properties are computed in ambient conditions. In Kim et al. [30], their predictive model is valid under the assumptions of high solid/fluid thermal conductivity ratio, sink dimensions much higher than fin dimensions, and laminar flow. The model has been validated for dimensionless pumping power and heat sink height, both defined in [30], between 5×10^9 and 10^{11}, and 1 and 2, respectively. In this study, we simulated values in between about 10^{11} and 10^{12}, and about 0.2 and 0.9. However, even if these ranges are outside the validated ones, it is straightforward to extend the validity of the correlations from Kim et al. [30] based on their model assumption.

All these terms listed are defined based on the following set of equations [30].

$$\eta_{eff} = \frac{\tanh\left[H \sqrt{\frac{h_c a_{sf}}{k_s (1-\varepsilon)}} \right]}{H \sqrt{\frac{h_c a_{sf}}{k_s (1-\varepsilon)}}} \tag{3}$$

$$K = \frac{\varepsilon w_c^2}{12[(0.289 + 16.0 w_c^*) + (0.00263 + 0.133 w_c^*) \mathrm{Re}_{w_c}]} \tag{4}$$

$$h_c = \frac{70 k_f}{17 w_c} \left[\left(17.4 w_c^* - 63.4 w_c^2 \right) + 7.67 \times 10^{-3} w_c^* \mathrm{Re}_{w_c} \right] \tag{5}$$

$$\varepsilon = \frac{w_c}{w_w + w_c} \tag{6}$$

$$a_{sf} = \frac{2}{w_w + w_c} \tag{7}$$

With $w_c{}^* = w_c/H$ as the dimensionless channel width, k_s as the solid phase thermal conductivity (aluminum), w_c as the fin spacing and w_w the fin thickness, already defined at the beginning of the present section. Reynolds number is defined by using the fin spacing as the characteristic length according to Kim et al. [30]. Since often the volumetric flow rate is the variable given by manufacturer, in cubic feet meters, the following relationship

have been used to link inlet velocity via the porosity with the volumetric flow rate after converting cfm in m^3/s.

$$u_{in} = \frac{\dot{V}_{in}}{\varepsilon L^2} \tag{8}$$

In this study, we assumed both number of fins N_{fins} and dimensionless fin thickness as input variables [28]. Therefore, fin typical geometrical equations that allow to relate all these variables are described from the following set of equations.

$$w_w = \frac{L}{N_{fins}+1} \Bigg/ \left(\frac{1-w_w^*}{w_w^*} + \frac{N_{fins}}{N_{fins}+1} \right) \tag{9}$$

$$w_c = w_w \frac{1-w_w^*}{w_w^*} = \frac{L - N_{fins} w_w}{N_{fins}+1} \tag{10}$$

$$w_w^* = \frac{w_w}{w_w + w_c} \tag{11}$$

With w_w* as the dimensionless fin thickness. With references to the device weight, just some geometrical considerations need to be done. The base volume is considered too in the computations by assuming a height of 6.40 mm. The following set of equations is used to characterize the device weight m_{sink} by including base volume and height too.

$$V_b = H_b L^2 \tag{12}$$

$$V_{fin} = w_w H L \tag{13}$$

$$m_{sink} = \left(V_b + N_{fins} V_{fin} \right) \rho_s \tag{14}$$

In this way, objective functions R_{th}, Δp and m_{sink} are computed from the aforementioned set of equations. Furthermore, we also underline that the present computations would not need to be validated since the employed correlations have been taken from studies which have been already validated. In our future plans, some more tests about optimum solutions that will be shown here would be really helpful to design the final heat sink.

2.3. Optimization Procedure

Because of the not so high computational effort and cost, a quite large amount of simulations can be done for the optimization procedure. Therefore, multi-objective optimization is implemented with a brute-force search approach in MATLAB with an in-house code. The total number of computations is equal to 12,800.

Objective functions have been shown in Section 2.2, while design variables are resumed in Table 1 by considering typical values of these applications. The fitness function discards solutions which are intended to be quite unrealistic, say the ones with $R_{th} > 1$ °C/W, $m_{sink} > 2$ kg and $\Delta p < 100$ Pa.

Table 1. Design variables ranges.

Design Variable	Symbol	Values		
		Min.	Step	Max.
Fins number	N_{fins}	8	2	24
Dimensionless fin thickness	w_w*	0.20	0.01	0.40
Volumetric flow rate (cfm)	$\dot{V}_{in}$	50	5	100
Sink height (mm)	H	20	10	100

3. Optimization Results

Results for multi-objective optimization are shown in this section. The 3D Pareto front is presented in Figure 2. In this figure, the optimum point calculated according to the

Utopia criterion [28] is highlighted too. In particular, this point allows to obtain R_{th} = 0.159, m_{sink} = 0.550 kg, and Δp = 14.99 Pa, by employing input variables equal to 24, 0.20, 50 cfm and 4 mm. In the figure, it is remarked that many points for the Pareto front have been obtained because non-dominant points are very few if one considers a three-objective function. In order to appreciate the relevance of the design variables, in Figure 3 input variables that allow to obtain Pareto front are resumed. From the figure, it can be seen that variables are quite spread in most of the cases, making multi-objective optimization useful to appreciate Pareto fronts. Among solutions, it is shown that Figure 2 (top-right) presents most of the scatters for lower values and also for the highest value investigated, similarly to what happens for Figure 2 (down-left). This could be attributed to the fact that there are three objective functions in contrast, thus extreme solutions could be dominant in the 3D space.

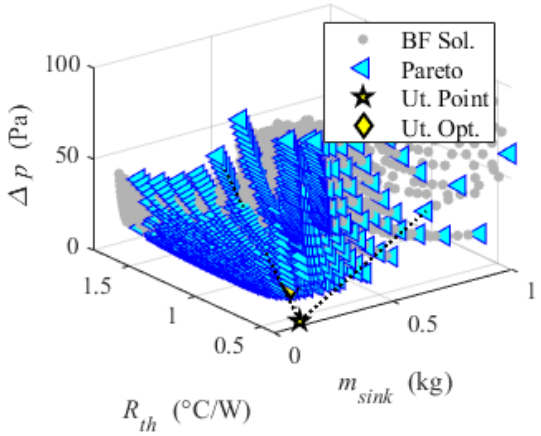

Figure 2. Optimized space of solutions for the three objective functions here investigated.

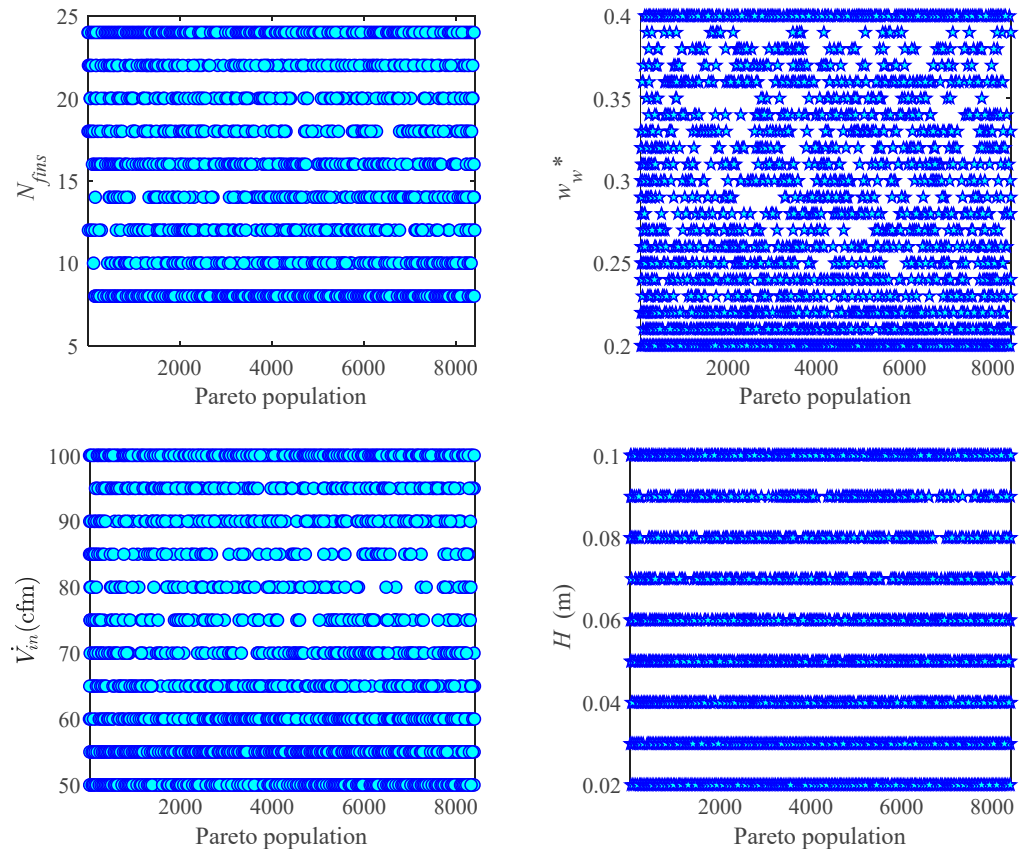

Figure 3. Design variables scatter points on the Pareto front.

In order to appreciate the relevance of each variable, 2D pareto fronts are reported in Figure 4. These fronts have been obtained by considering two objective functions per time. Because the BF approach is employed, which in turn simulates all the combinations, it is supposed to not be necessary to run again the code because of the very large number of individuals simulated. In all the cases, one can remark that Pareto fronts are quite regular, with a more or less hyperbolic trend. Utopia optima have been obtained with 0.184 °C/W and 0.399 kg (Figure 4, top-left), 0.461 kg and 20.68 Pa (Figure 4, top-right), and 0.135 °C/W and 12.46 Pa (Figure 4, down). These values are slightly different from the Utopia optimum obtained for the 3D case, making it useful to consider the three-objective functions together. However, using 2D pareto fronts for optima analysis might be reasonable if one wants to just consider two out of three objective functions in its study.

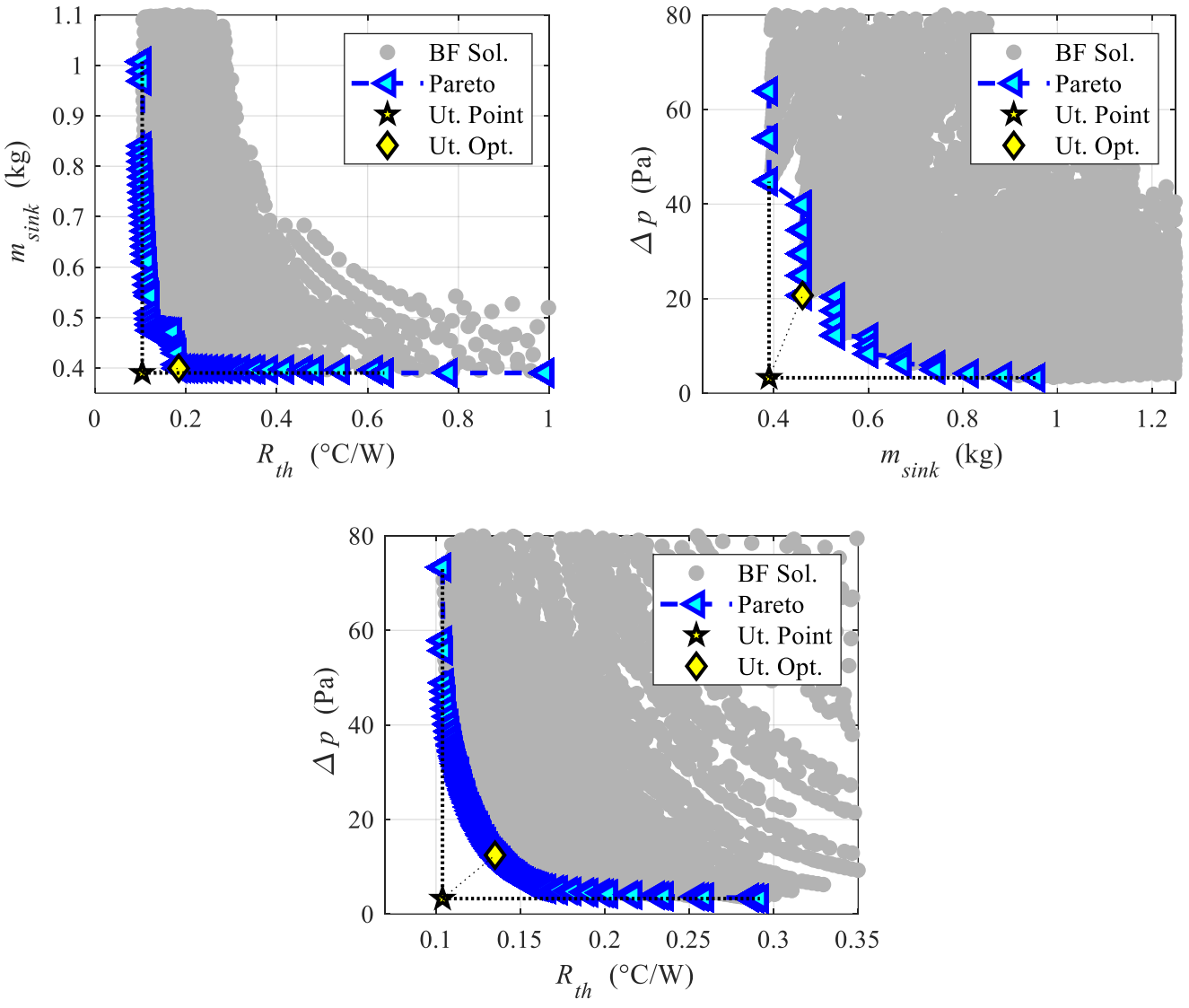

Figure 4. 2D Solutions extrapolated from 3D solutions for different couples of objective functions.

4. Predictive Models

Starting from the large bunch of cases here simulated, a set of correlations for whom wants to design these devices have been obtained too. In particular, two approaches have been followed. The first is based on conventional linear regression analyses, while the second is on artificial neural networks. By considering the $F_j(x)$ objective function, with j = 1, 2 and 3, the following generic function is considered.

$$y = a_1 + b_1x_1 + b_2x_2 + b_3x_3 + b_4x_4 \quad (15)$$

$$y_p = a_1 + b_1x_{1,p} + b_2x_{2,p} + b_3x_{3,p} + b_4x_{4,p} \quad (16)$$

With the design variables x_i labelled as vectors x_1, x_2, x_3 and x_4. The second equation, Equation (16), reported with subscript p, which stands for Pareto, is obtained just to analyze the quality of the predictions by making references only to the Pareto front design variables. Regression coefficients are the same of the overall analysis in order to include more datapoints. In other words, it is just verified how much a generic correlation works for the Pareto front case. Comparison between simulated and predicted values is shown in Figure 5 for all the j-objective functions analyzed. It is clear that the second objective function, that is the weight, provides the best agreement because of the simplicity of the problem. In the regression, some variables that do not affect the weight like the fan mass flow rate are included; thus, making predictions better because they did not have any relevant effect on the considered objective function. In order to appreciate the quality of the regression, coefficient of determination R^2, *RMSE* and *MAPE* are resumed in Table 2 for both overall design variables and Pareto front design variables. From the table, it is clear that the second objective function present the best values by far.

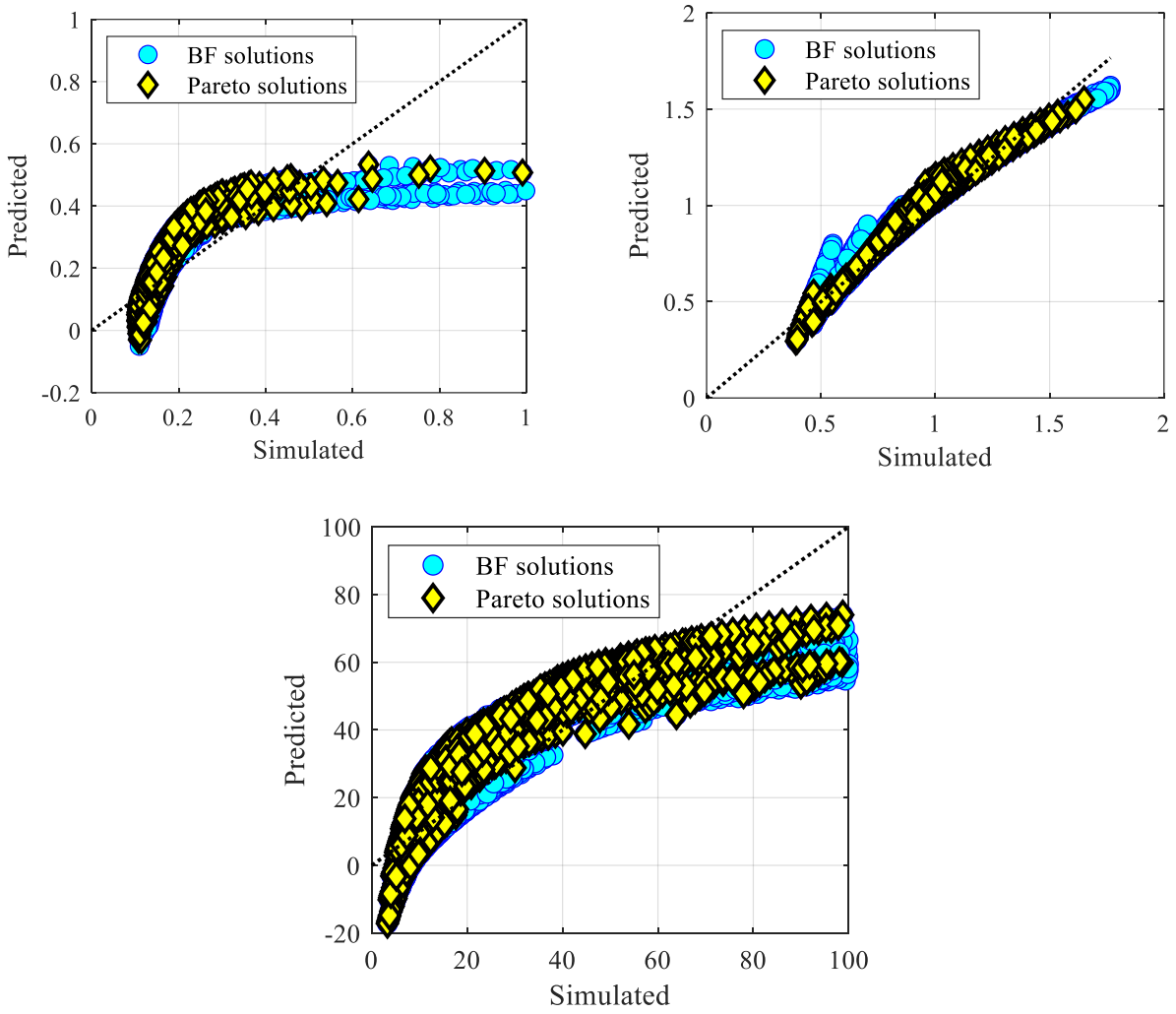

Figure 5. Comparisons between predicted (multiple−linear regression) and simulated solutions for both BF and Pareto solutions the three different objective functions investigated (j = 1, 2, and 3, from the left, to the right, to the bottom).

Table 2. Statistical regression parameters for the various objective functions referred to both design variables and Pareto front design variables.

$F_j(x)$	R^2		RMSE		MAPE	
R_{th} (°C/W)	x_i	$x_{i,p}$	x_i	$x_{i,p}$	x_i	$x_{i,p}$
	0.62	0.67	0.12	0.14	40.6	37.3
m_{sink} (kg)	x_i	$x_{i,p}$	x_i	$x_{i,p}$	x_i	$x_{i,p}$
	0.96	0.94	0.08	0.07	8.51	11.4
Δp (Pa)	x_i	$x_{i,p}$	x_i	$x_{i,p}$	x_i	$x_{i,p}$
	0.75	0.72	12.3	13.3	57.2	75.5

Because of the low quality of the linear regressions, in this work regression analysis has been done by employing artificial neural networks. The neural network employed is a two-layer feed-forward network, with sigmoid hidden neurons and linear output neurons. Training, Validation and Test sample sets have been set equal to 70%, 15% and 15%. Neural networks have been reconstructed by using the Levenberg-Malquardt algorithm to minimize the *MSE*, with a convergence criterion of 8.82×10^{-7}, 2.77×10^{-8} and 3.42×10^{-3} to be reached after 1000 epochs. Ten single-layered neurons have been used for such predictions, and weights extrapolated that allow to reconstruct the neural network are resumed in Table 3. Offset and gain for the input values are always equal to 8, 0.2, 50, 0.02, and 0.125, 10, 0.04, 25, respectively. Minimum y value is always set equal to -1 for both input and output. Gain and offset on the first output are 2.2362 and 0.1038 for the first objective function, 1.4536 and 0.3902 for the second, and finally 0.0207 and 3.2689 for the third one. Comparisons between simulated and predicted values are shown in Figure 6, showing a really good agreement with this approach.

Table 3. Bias and weights for the neural networks here trained.

$F_j(x)$	1st Layer					2nd Layer	
	Bias	Weights				Bias	Weights
R_{th} (°C/W)	−2.5674	−0.3525	−0.0211	−0.1449	−0.0493	20.7259	12.4699
	−1.0418	0.2968	0.0782	−0.8206	0.0389		0.0290
	−0.5616	−0.0735	−1.3042	−0.1028	−1.0500		0.0069
	−16.1835	−2.2422	−0.7783	−0.8330	−13.0148		8.3386
	4.2947	1.4565	0.1470	0.4373	0.8708		−4.2753
	11.0239	2.4059	0.7746	0.9278	7.7712		17.7774
	−4.4437	−0.5398	−0.1854	−0.1947	−2.5363		4.7389
	23.3584	6.0179	1.7070	2.2244	16.9360		−1.5910
	−9.9535	−2.4806	−0.7398	−0.9489	−7.0125		6.9171
	2.2930	−0.0075	0.2280	0.0118	−0.3560		−1.2040
m_{sink} (kg)	1.1146	−0.0039	−0.4664	−0.0001	0.1694	0.5166	2.5372
	0.0864	−0.0390	0.4804	0.0004	−0.1044		−1.7277
	1.0744	−0.0083	−0.3883	−0.0002	−0.1497		−3.7465
	−0.4097	0.5734	−1.1600	0.0541	−1.4248		0.0002
	−0.0831	−0.1258	−0.3873	−0.0012	−0.2836		−0.2674
	−0.1018	0.0452	−0.4148	−0.0002	−0.0199		−2.2446
	−0.9336	−0.7900	−0.1614	0.0046	0.5151		−0.0305
	1.4079	0.8178	−1.1347	−0.0347	−1.6955		0.0023
	2.0536	1.4128	1.2713	−1.5553	0.8827		−0.0001
	−2.9055	−1.9424	0.1259	0.0024	0.6136		−0.0472
Δp (Pa)	5.2759	−0.0365	−0.1817	−0.7438	4.8688	4.6150	−1.6469
	2.7637	−0.0502	−0.0764	−0.9897	3.3145		−0.2119
	−1.0387	0.0084	−0.2049	0.6033	−0.5076		2.0768
	−1.7708	0.2673	0.3438	0.2695	0.0447		2.3314
	0.5079	−0.0205	0.0234	−0.3561	0.9547		2.5127
	−0.5778	0.1753	0.1217	0.1263	−0.0026		3.2698
	2.7824	−0.0308	−0.3278	−0.2709	1.1301		−7.7190
	0.6964	−0.0194	0.0513	−0.4127	0.7985		−7.3309
	0.9049	−0.0181	0.1210	−0.4997	0.6177		6.7696
	1.2250	−0.1505	−0.1117	−0.0781	−0.0009		9.6981

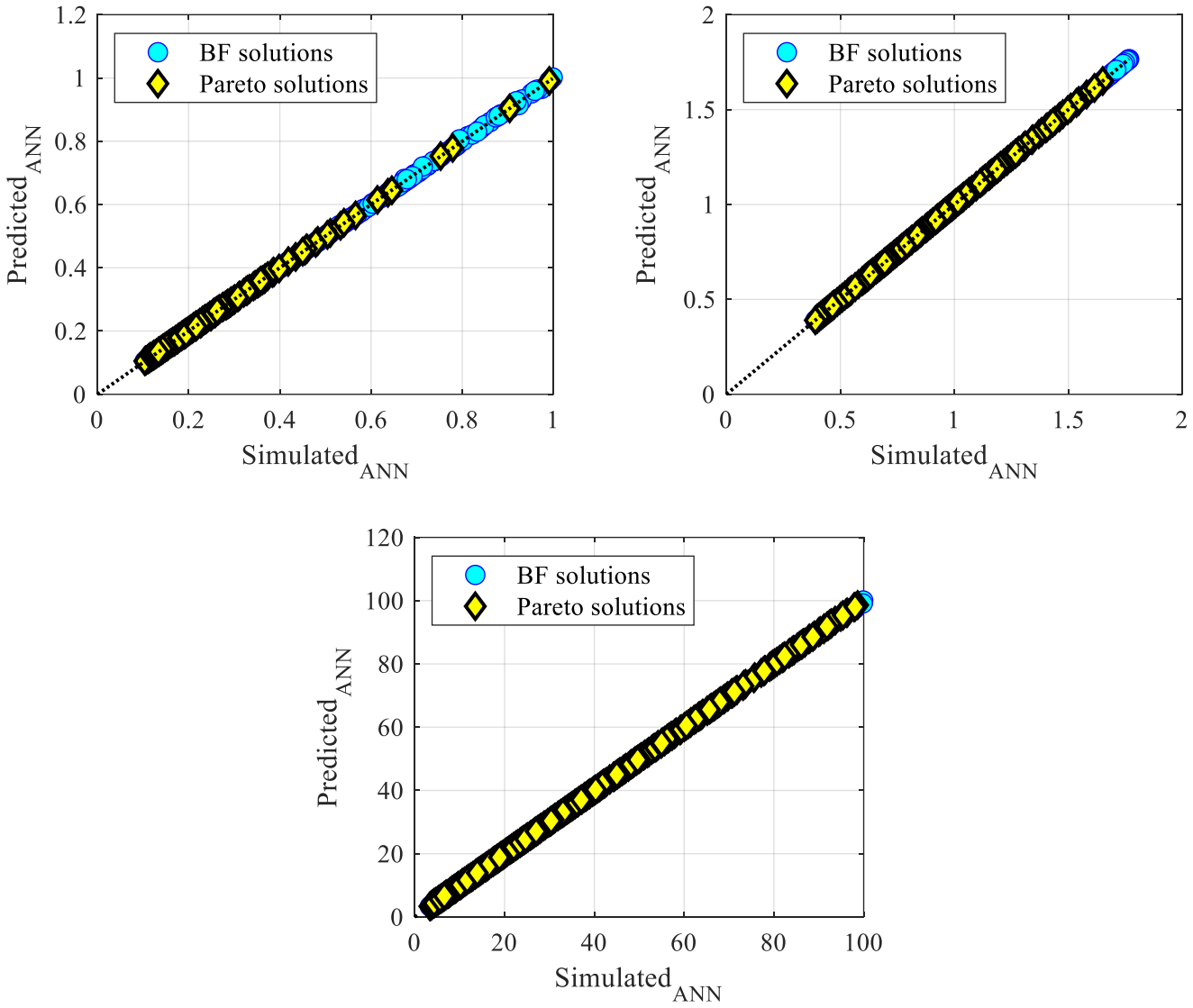

Figure 6. Comparisons between predicted (artificial neural network) and simulated solutions for both BF and Pareto solutions the three different objective functions investigated (j = 1, 2, and 3, from the left, to the right, to the bottom).

5. Conclusions

In the present contribution, a brute-force three-objective optimization of thermal resistance, weight and pressure drop, has been carried out on an impinging-flow finned heat sink to be used on a Peltier cell for storage of biomedical products. The fitness function to run the algorithm is built up by employing well-established heat transfer and pressure drop correlations from the literature. Fin numbers, heights and thicknesses, as well as volumetric flow rate to design the fan, have been chosen as design variables. The optimization here performed provides criterion to design these devices depending on the preferred criterion among the investigated objective functions. Based on the Utopia optimum criterion, an optimum of R_{th} = 0.159, m_{sink} = 0.550 kg, and Δp = 14.99 Pa, is here achieved. If one just considers two objective functions, Utopia optimum have been obtained with values of 0.184 °C/W and 0.399 kg, 0.461 kg and 20.68 Pa, and 0.135 °C/W and 12.46 Pa. Finally, in order to provide who wants to design such devices of a practical instrument, correlations between design variables and objective functions have been derived based on either multiple linear regressions or artificial neural networks. In particular, the latter approach provides very high values for typical statistical coefficients as well as the R^2. This means that, based

on weight and biases provided in this work, one could select the design variables that allow to derive some values from constrained objective functions.

Author Contributions: Conceptualization: L.G., M.I. and G.M.M.; Methodology: M.I. and G.M.M.; Software, validation, formal analysis, investigation, resources, visualization, and data curation: M.I. and G.M.M.; Writing—original draft preparation: M.I. and G.M.M.; Writing—review and editing: L.G., M.I. and G.M.M.; Supervision, project administration, and funding acquisition: L.G. All authors have read and agreed to the published version of the manuscript.

Funding: This work was supported by Carpitech Srl.

Data Availability Statement: Data of the present research are available upon request to the authors.

Conflicts of Interest: The authors declare no conflict of interest.

Nomenclature

a, b	regression coefficients
a_{sf}	specific surface area (1/m)
c_p	specific heat capacity (J/kg K)
$F_j(x)$	objective function
h_c	heat transfer coefficient (W/m^2 K)
k	thermal conductivity (W/m K)
K	permeability (m^2)
H	height (m)
L	length (m)
m_{sink}	mass (kg)
N_{fins}	fin numbers
p	pressure (Pa)
$\dot{Q}$	heat rate (W)
Re	Reynolds number
R_{th}	thermal resistance (°C/W)
T	temperature (K)
u_{in}	inlet velocity (m/s)
$\dot{V}_{in}$	volumetric flow rate (m^3/s)
V_{fin}	fin volume (m^3)
V	volume (m^3)
w_c	fin spacing (m)
w_w	fin thickness (m)
x	Regressions inputs
y	Regression output
Greek letters	
ε	porosity
h_{eff}	fin efficiency
ρ	density (kg/m^3)
Subscripts	
b	base
f	fluid
s	solid
Superscripts	
*	dimensionless

References

1. European Commission Guidelines on Good Distribution Practice of Medicinal Products for Human Use (94/C63/03). Available online: https://eur-lex.europa.eu/legal-content/EN/TXT/?uri=uriserv%3AOJ.C_.1994.063.01.0004.01.ENG&toc=OJ%3AC%3A1994%3A063%3ATOC (accessed on 15 September 2022).
2. Taylor, J. Recommendations on the control and monitoring of storage and transportation temperatures of medicinal products. *Pharm. J.* **2001**, *267*, 128–131.
3. Shukla, A.; Sharma, A.; Shukla, M.; Chen, C.R. Development of thermal energy storage materials for biomedical applications. *J. Med. Eng. Technol.* **2015**, *39*, 363–368. [CrossRef] [PubMed]

4. Valeri, C.R.; Pivacek, L.E. Effects of the temperature, the duration of frozen storage, and the freezing container on in vitro measurements in human peripheral blood mononuclear cells. *Transfusion* **1996**, *36*, 303–308. [CrossRef] [PubMed]
5. Massie, I.; Selden, C.; Hodgson, H.; Fuller, B. Storage temperatures for cold-chain delivery in cell therapy: A study of alginate-encapsulated liver cell spheroids stored at −80 °C or −170 °C for up to 1 year. *Tissue Eng. Part C Methods* **2013**, *19*, 189–195. [CrossRef] [PubMed]
6. Shafaat, K.; Hussain, A.; Kumar, B.; Hasan, R.; Prabhat, P.; Yadav, V. An overview: Storage of pharmaceutical products. *World J. Pharm. Pharm. Sci.* **2013**, *2*, 2499–2515.
7. Uddin, M.N.; Roni, M.A. Challenges of storage and stability of mRNA-based COVID-19 vaccines. *Vaccines* **2021**, *9*, 1033. [CrossRef] [PubMed]
8. Khan, A.Z.; Utheim, T.P.; Jackson, C.J.; Tønseth, K.A.; Eidet, J.R. Concise Review: Considering Optimal Temperature for Short-Term Storage of Epithelial Cells. *Front. Med.* **2021**, *8*, 686774. [CrossRef] [PubMed]
9. Indirani, S.; Arjunan, S. Selection and synthesis of thermal energy storage PCM with silicon carbide for biomedical applications. *Appl. Nanosci.* **2022**, *46*, 1–8. [CrossRef]
10. Ray, A.K.; Singh, S.; Rakshit, D.; Udayraj. Comparative study of cooling performance for portable cold storage box using phase change medium. *Therm. Sci. Eng. Prog.* **2022**, *27*, 101146. [CrossRef]
11. Lloyd, J.; Lydon, P.; Ouhichi, R.; Zaffran, M. Reducing the loss of vaccines from accidental freezing in the cold chain: The experience of continuous temperature monitoring in Tunisia. *Vaccine* **2015**, *33*, 902–907. [CrossRef]
12. Junghanss, T.; Boock, A.U.; Vogel, M.; Schuette, D.; Weinlaeder, H.; Pluschke, G. Phase Change Material for Thermotherapy of Buruli Ulcer: A Prospective Observational Single Centre Proof-of-Principle Trial. *PLOS Negl. Trop. Dis.* **2009**, *3*, e380. [CrossRef]
13. World Health Organization. Temperature Monitors for Vaccines and the Cold Chain: Cold-Chain Monitor, Vaccine Vial Monitor, Freeze Watch, Stop! Watch, DT and TT Shipping Indicator. 1999. Available online: https://apps.who.int/iris/handle/10665/65964 (accessed on 15 September 2022).
14. World Health Organization. Cool Innovations for Vaccine Transportation and Storage. 2012. Available online: http://www.path.org/publications/files/TS_opt_cool_innov.pdf (accessed on 15 September 2022).
15. Ma, K.; Zhang, X.; Ji, J.; Han, L.; Ding, X.; Xie, W. Application and research progress of phase change materials in biomedical field. *Biomater. Sci.* **2021**, *9*, 5762–5780. [CrossRef]
16. Rokde, K.; Patle, M.; Kalamdar, T.; Gulhane, R.; Hiware, R. Peltier Based Eco-Friendly Smart Refrigerator for Rural Areas. *Int. J. Adv. Res. Comput. Sci. Softw. Eng.* **2017**, *7*, 718–721. [CrossRef]
17. Chaudhari, V.; Kulkarni, M.; Sakpal, S.; Ubale, A.; Sangale, A. Eco-Friendly Refrigerator Using Peltier Device. In Proceedings of the 2018 International Conference on Communication and Signal Processing (ICCSP), Chennai, India, 3–5 April 2018.
18. Yadav, H.; Srivastav, D.; Kumar, G.; Yadav, A.K.; Goswami, A. Experimental Investigations and Analysis of Thermoelectric Refrigerator with Multiple Peltier Modules. *Int. J. Trend Sci. Res. Dev.* **2019**, *3*, 1337–1340. [CrossRef]
19. Rapaka, S.; Bobba, N.S.N.; Penigandla, G.S.; Dondapati, R.S. Thermohydraulic Management of Batteries with the help of the Peltier Cell for Automotive and Space Applications. *IOP Conf. Ser. Mater. Sci. Eng.* **2022**, *1248*, 012017. [CrossRef]
20. Lucas, S.; Bari, S.; Marian, R.; Lucas, M.; Chahl, J. Cooling by Peltier effect and active control systems to thermally manage operating temperatures of electrical Machines (Motors and Generators). *Therm. Sci. Eng. Prog.* **2022**, *27*, 100990. [CrossRef]
21. De Mey, G.; Kos, A.; Górecki, K. Optimal Temperature Regulation of Integrated Circuits with Peltier Heat Pumps. *Energies* **2022**, *15*, 1125. [CrossRef]
22. Heredia-Aricapa, Y.; Belman-Flores, J.M.; Soria-Alcaraz, J.A.; Pérez-García, V.; Elizalde-Blancas, F.; Alfaro-Ayala, J.A.; Ramírez-Minguela, J. Multi-Objective Optimization of a Multilayer Wire-on-Tube Condenser: Case Study R134a, R600a, and R513A. *Energies* **2022**, *15*, 6101. [CrossRef]
23. Grygierek, K.; Ferdyn-Grygierek, J. Multi-Objective Optimization of the Envelope of Building with Natural Ventilation. *Energies* **2018**, *11*, 1383. [CrossRef]
24. Ferreira, A.C.; Silva, A.; Teixeira, J.C.; Teixeira, S. Multi-Objective Optimization of Solar Thermal Systems Applied to Portuguese Dwellings. *Energies* **2020**, *13*, 6739. [CrossRef]
25. Ndao, S.; Peles, Y.; Jensen, M.K. Multi-objective thermal design optimization and comparative analysis of electronics cooling technologies. *Int. J. Heat Mass Transf.* **2009**, *52*, 4317–4326. [CrossRef]
26. Karathanassis, I.K.; Papanicolaou, E.; Belessiotis, V.; Bergeles, G.C. Multi-objective design optimization of a micro heat sink for Concentrating Photovoltaic/Thermal (CPVT) systems using a genetic algorithm. *Appl. Therm. Eng.* **2013**, *59*, 733–744. [CrossRef]
27. Imran, M.; Pambudi, N.A.; Farooq, M. Thermal and hydraulic optimization of plate heat exchanger using multi objective genetic algorithm. *Case Stud. Therm. Eng.* **2017**, *10*, 570–578. [CrossRef]
28. Bianco, N.; Iasiello, M.; Mauro, G.M.; Pagano, L. Multi-objective optimization of finned metal foam heat sinks: Tradeoff between heat transfer and pressure drop. *Appl. Therm. Eng.* **2021**, *182*, 116058. [CrossRef]
29. Feng, S.S.; Kuang, J.J.; Wen, T.; Lu, T.J.; Ichimiya, K. An experimental and numerical study of finned metal foam heat sinks under impinging air jet cooling. *Int. J. Heat Mass Transf.* **2014**, *77*, 1063–1074. [CrossRef]
30. Kim, D.-K.; Kim, S.J.; Bae, J.-K. Comparison of thermal performances of plate-fin and pin-fin heat sinks subject to an impinging flow. *Int. J. Heat Mass Transf.* **2009**, *52*, 3510–3517. [CrossRef]